PCCP

Cite this: *Phys. Chem. Chem. Phys.*, 2011, **13**, 14462–14465

www.rsc.org/pccp

COMMUNICATION

Fabrication of Co_3O_4-reduced graphene oxide scrolls for high-performance supercapacitor electrodes†

Weiwei Zhou,[a] Jinping Liu,[ab] Tao Chen,[c] Kim Seng Tan,[a] Xingtao Jia,[a] Zhiqiang Luo,[a] Chunxiao Cong,[a] Huanping Yang,[a] Chang Ming Li[c] and Ting Yu*[ad]

Received 20th April 2011, Accepted 23rd June 2011
DOI: 10.1039/c1cp21917k

A new type of scrolled structure of Co_3O_4/reduced graphene oxide (r-GO) is facilely prepared through a two-step surfactant-assisted method. This assembly enables almost every single Co_3O_4 scroll to connect with the r-GO platelets, thus leading to remarkable electrochemical performances in terms of high specific capacitance and good rate capability.

In recent years, with the impending exhaustion of fossil fuels reserves and the rising global demand for energy, the effort to maximize the utilization of present energy sources and search for alternative energy storage devices has intensified dramatically.[1–3] Supercapacitors, as an intermediate system between dielectric capacitors and batteries, have drawn significant attention due to their superb characteristics of high power density and long cycle life.[4–6] In general, the energy storage is either capacitive or pseudocapacitive in nature, based on which supercapacitors can be classified into electrical double-layer capacitors (EDLCs) and pseudocapacitors.[2] EDLCs using carbon-based materials usually have high power density but suffer from low capacitance.[5,7,8] In contrast, pseudocapacitors, employing transition metal oxides, hydroxides, and conducting polymers could provide high specific capacitance but suffer from high cost and poor cycling stability arising from their low conductivity.[9,10] As a result, superior performance is expected from the integration of metal oxides/hydroxides and carbon-based materials.[11]

Graphene, as a single-atom-thick carbon material, shows many advantages for growing and anchoring metal oxides in view of its large surface area, good electrical conductivity, high flexibility, and mechanical strength. Recent works have reported the use of metal oxides coupled with different graphene derivatives in energy storage applications, such as Li-ion battery and supercapacitor, all of which have demonstrated improved performances originating from enhanced electron transport rate, high electrolyte contact area, or structural stability.[12–17] Although various metal oxides have been incorporated with graphene, the basic combination mode can be interpreted as metal oxides attached onto the surface or intercalated into the interlayer of large patches of graphene-based materials.[12,13,15,18–22] Very recently, Yang *et al.* developed a fresh integration mode by encapsulating metal oxide nanoparticles with graphene sheets, the process of which was driven by the mutual electrostatic interactions between negatively charged graphene oxide (GO) and positively charged oxide nanoparticles.[23] This assembly enables a novel integration of electrochemically active metal oxide nanoparticles with graphene sheets, hence leading to remarkable lithium storage performance.

Here, we report another new hybridization mode between graphene and metal oxides by integrating the reduced graphene oxide (r-GO) platelets into the Co_3O_4 scrolls. Our strategy is assisted by the lamellar micelles of the surfactant and subsequent post-annealing. Rather than serving as the supporting substrates for guest materials in most cases, r-GO platelets are incorporated into nearly every single Co_3O_4 scroll and are believed to connect with Co_3O_4 through the residual oxygen functional groups on their basal planes and the edges. The resulting Co_3O_4/r-GO exhibits a large specific capacitance of 163.8 F g^{-1} at a current density of 1 A g^{-1}, which is about 13 times higher than that of pure Co_3O_4. We attribute this improvement to the synergetic effect between the r-GO platelets and Co_3O_4 as well as the unique scrolled structure of Co_3O_4/r-GO. Our results suggest a novel integration mode between metallic and carbonaceous species, which opens up a new approach for graphene to boost the energy storage property.

The overall synthetic procedure of the Co_3O_4/r-GO scrolls involves two steps: (i) obtaining the CoC_2O_4/GO scroll precursor at room temperature with the assistance of sodium dodecyl sulfate (SDS) in a mixed solvent; (ii) phase transition from CoC_2O_4 to Co_3O_4 ($3CoC_2O_4 \rightarrow Co_3O_4 + 2CO_2\uparrow + 4CO\uparrow$) and simultaneous partial reduction of GO by a post-annealing treatment of the precursor at 450 °C for 2 h under argon

[a] *Division of Physics and Applied Physics, School of Physical and Mathematical Sciences, Nanyang Technological University, 21 Nanyang Link, 637371, Singapore. E-mail: yuting@ntu.edu.sg*
[b] *Institute of Nanoscience and Nanotechnology, Department of Physics, Central China Normal University, Wuhan, 430079, P. R. China*
[c] *School of Chemical and Biomedical Engineering, Nanyang Technological University, 70 Nanyang Drive, 637457, Singapore*
[d] *Department of Physics, Faculty of Science, National University of Singapore, 117542, Singapore*

† Electronic supplementary information (ESI) available: Experimental section, XRD pattern, SEM images, Optical images and Raman spectrum, Electrochemical property. See DOI: 10.1039/c1cp21917k

protection [see ESI† for details]. The GO was prepared by a modified Hummers method.[24,25] Mainly, small GO platelets in the upper suspension were employed for our experiments. Tapping-mode atomic force microscope (AFM) images demonstrate that these GO platelets exist as one-layer carbon sheets (Fig. S1, ESI†).[26,27] The purities of both the CoC_2O_4/GO precursor and the final product Co_3O_4/r-GO are revealed by their corresponding XRD patterns (Fig. S2, ESI†). Fig. 1a shows the SEM image of typical CoC_2O_4/GO precursor scrolls. The average length and diameter of the scrolls are about 2 μm and 800 nm, respectively. Fig. 1b shows the TEM image of a single CoC_2O_4/GO scroll. Through close inspection under TEM, we can even observe the GO platelet at the end of the scroll (indicated by the circle in the inset of Fig. 1b). It can be seen that the scrolls are in fact composed of sub-nanorods, which are stacked in a parallel fashion. A low-magnification SEM image including a large amount of scrolls further indicates the high yield and uniformity (Fig. S3, ESI†). Unlike most carbon nanoscrolls which are rolled up from one side of the mother sheet,[28,29] the present composite scrolls are rolled up from both sides. Raman characterization can detect the signals of GO in almost every single CoC_2O_4/GO scroll (Fig. S4, ESI†). Moreover, GO is observed to distribute all over the whole scrolled structure or even extend outside the main body of a CoC_2O_4 scroll (Fig. 1c–e and Fig. S5, ESI†).

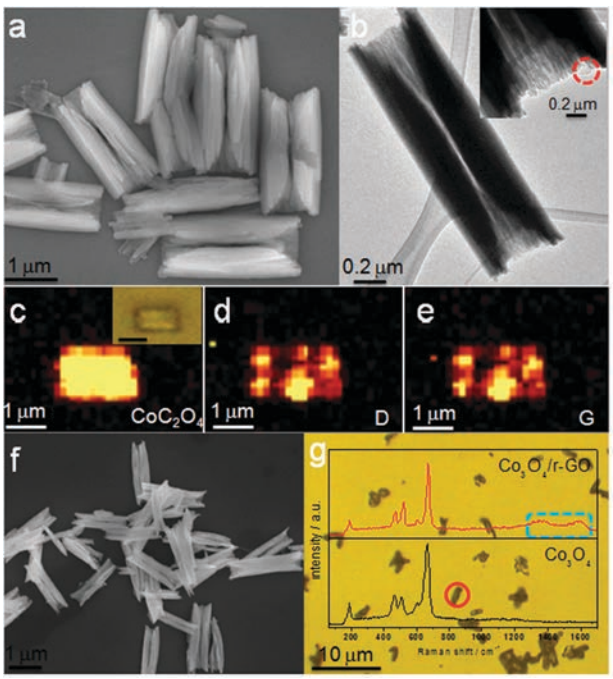

Fig. 1 (a) SEM image of the CoC_2O_4/GO scrolls. (b) TEM image of a single CoC_2O_4/GO scroll; inset shows the high-magnification TEM image. (c–e) Raman mapping images of CoC_2O_4 and D, G bands of GO for a single CoC_2O_4/GO scroll; inset in (c) shows the optical image of the selected CoC_2O_4/GO scroll. The scale bar of the inset is 1 μm. (f) SEM image of the Co_3O_4/r-GO scrolls. (g) Optical image of the Co_3O_4/r-GO scrolls and Raman spectra of pure Co_3O_4 (for reference) and Co_3O_4/r-GO obtained from a single scroll marked by a red circle in the optical image. The Raman signals of r-GO are highlighted with a blue dashed rectangular box.

Heat treatment is conducted subsequently to obtain the active transition metal oxide product. Despite the phase transition from CoC_2O_4 to Co_3O_4, the overall scroll morphology and the presence of GO can be preserved after annealing (Fig. 1f and g).

Layered structures, as proven to be the basis for the formation of the scrolls, can originate from either the target material itself or soft templates (*e.g.* surfactant, organic molecule).[30–35] The results of a control experiment conducted without GO still show the presence of the scroll morphology (Fig. S6a, ESI†), whereas in another control experiment, in the absence of the SDS, only nanorod clusters have been formed (Fig. S6b, ESI†). Thus, the possibility of GO serving as the template for the formation of scrolled structures is ruled out. Instead, the surfactant SDS used in this system must play a constructive role in determining the final scrolled structure of CoC_2O_4. Fig. 2 illustrates the suggested growth mechanism of the CoC_2O_4/GO scrolls. Herein, the SDS is believed to form lamellar micelles in the solution ready for the subsequent growth of the scrolls. (The lamellar micelles should have periodically layered structures. However, for simplicity, we only show monolayer structures in Fig. 2.) With reference to the diagrams in Fig. 2, we describe three cases in the formation of the CoC_2O_4 scrolls in the absence and presence of graphene derivatives. Firstly, in the case where no graphene derivatives are present (left column in Fig. 2: SDS), the CoC_2O_4 precursor is first nucleated on the lamellar micelles of the SDS due to the electrostatic interaction between Co^{2+} cations and anion groups on the SDS. Subsequently, anisotropic growth, which is accompanied by the rolling process, occurs. We attribute this rolling to a kinetically driven process rather than a thermodynamically driven one as the reaction takes place at room temperature. One possibility is proposed on the basis of the following two steps:[30,31] (1) under vigorous magnetic stirring, the lamellar micelles become loose at the edges; (2) the rolling happens due to the structural stress caused by the gravity differences of the CoC_2O_4 between the edges and the centre as well as the interactions between the hydrophobic

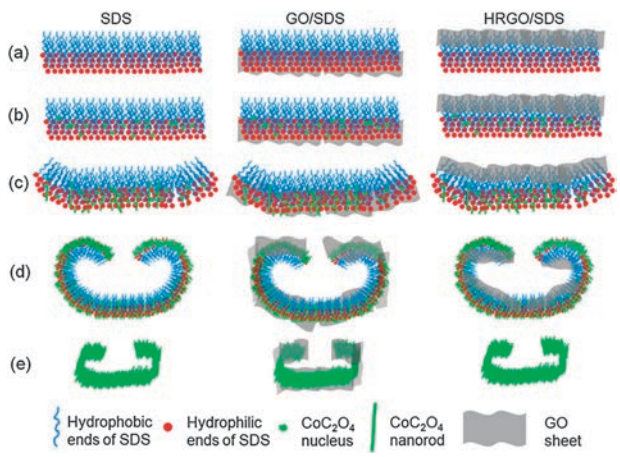

Fig. 2 Schematic diagram showing the formation of the CoC_2O_4 scrolls in the absence and presence of graphene derivatives. (a)–(e) represent the typical reaction stages of the formation of the lamellar micelles of the surfactant, nucleation of CoC_2O_4, initial growth of CoC_2O_4 nanorods, rolling process and washing away the surfactant, respectively.

ends of the SDS in the same layer. The neighboring layers of an SDS micelle are believed to roll up to the same direction due to the connection of Co^{2+} cations between them. The bending direction is determined by the layer with stronger force. The investigation of the exact mechanism for this rolling process is going on. Secondly, in the case where GO is present (middle column in Fig. 2: GO/SDS), the GO is added after the dissolution of SDS, sonicated for 30 min. In this regard, it could be attached onto the hydrophilic ends of the SDS. After the SDS is washed away, the presence of GO in the scrolls is to a large extent due to the ionic bonding between the oxygen functional groups on the GO platelets and Co^{2+} cations (Fig. S4, ESI†). In order to further confirm the connection between GO and CoC_2O_4, a control experiment is conducted where GO is present without the SDS. Despite not having any more scrolled structures formed (Fig. S6b, ESI†), the Raman signals of GO can still be detected in almost every single CoC_2O_4 cluster after being washed with water and ethanol for several times (Fig. S7, ESI†). Therefore, there is certain interaction between the GO platelets and CoC_2O_4. Ionic bonding between the oxygen functional groups on the GO platelets and Co^{2+} cations is of high possibility the interaction between GO and CoC_2O_4. Thirdly, for the case with hydrogen reduced GO (HRGO, in order to distinguish from the partially reduced GO obtained in the second-step annealing in Ar, we use HRGO to stand for high-temperature hydrogen reduced GO) (right column in Fig. 2: HRGO/SDS), the absence of oxygen functional groups leads HRGO platelets to only have hydrophobic interaction with the alkylated chains of the SDS but without any interaction with CoC_2O_4. In contrast to the second case, SDS here is indeed the bridge linking HRGO and CoC_2O_4. Hence, most HRGO platelets are expected to be removed after the SDS template is washed away. As we have expected, even when Raman characterization is conducted on a large scale of CoC_2O_4 scrolls, the Raman signals of HRGO are either absent or very weak (Fig. S8, ESI†).

Cyclic voltammetry (CV) and galvanostatic charge–discharge measurements are conducted in a three-electrode cell to evaluate the electrochemical properties of the Co_3O_4/r-GO scrolls. Although the three-electrode cell would overstate the specific capacitance compared with a two-electrode cell, it can still be used to investigate the electrochemical behaviour of a single electrode.[36,37] Fig. 3a presents the representative CV curves of the Co_3O_4/r-GO scrolls at different scan rates in a 6 M KOH electrolyte. The largest specific capacitance (SC) of 159.8 F g^{-1} can be reached at a scan rate of 5 mV s^{-1}, which is quite consistent with the largest value (163.8 F g^{-1}, at 1 A g^{-1}) calculated from the charge–discharge curves (Fig. 3b). In addition, when the current density is increased from 1 A g^{-1} up to 10 A g^{-1}, the SC can still remain at a high level above 140 F g^{-1} with a good retention of about 87% (Fig. 3b). For comparison, bare Co_3O_4 scrolls are also tested under the same electrochemical conditions (Fig. S9a, ESI†). It is striking to note that, after introduction of partially reduced GO to pristine Co_3O_4 scrolls, the area surrounded by the CV curve becomes significantly large (Fig. 3c). The nearly rectangular shape of the CV curve implies the good capacitive behaviour of the composite. The SC of the Co_3O_4/r-GO composite is calculated to be as large as 11 times of that of pristine Co_3O_4 at

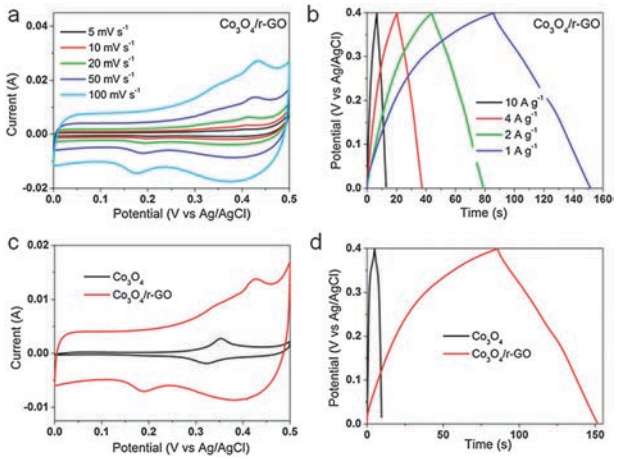

Fig. 3 (a, b) CV and galvanostatic charge–discharge curves of the Co_3O_4/r-GO composite electrode at different scan rates and current densities in a 6 M KOH electrolyte, respectively. (c) CV curves of pure Co_3O_4 and Co_3O_4/r-GO at a scan rate of 50 mV s^{-1}. (d) Galvanostatic charge–discharge curves of the Co_3O_4 and Co_3O_4/r-GO at a current density of 1 A g^{-1}.

different scan rates (Table S1 in the ESI†). As aforementioned, the integration of carbonaceous material and metal oxide is of hope to boost the energy storage performance. Herein, the high SC of the composite is believed to stem from the combination of the EDL capacitance and pseudocapacitance from r-GO platelets and Co_3O_4, respectively. Another noteworthy feature of the Co_3O_4/r-GO composite is its good rate capability. The discharge time of Co_3O_4/r-GO at 10 A g^{-1} (6.3 s) is even longer than that of bare Co_3O_4 at 1 A g^{-1} (4.6 s, Fig. 3d).

To further reveal the function of r-GO platelets in the Co_3O_4/r-GO scrolls, we simply prepared another Co_3O_4/carbon black (CB) composite by mechanical blending for comparison, where the amount of CB is equal to that of r-GO. The SC of the mixed Co_3O_4/CB composite calculated from its CV curve is about 52 F g^{-1} (Fig. S9b, ESI†). This value, albeit two times higher than that of pure Co_3O_4 (12.9 F g^{-1}), is much lower than that of Co_3O_4/r-GO (131.2 F g^{-1}). The possible reason is the poor distribution of CB in the Co_3O_4 scrolls caused by mechanical blending. However, the fast current response can be observed for both Co_3O_4/r-GO and Co_3O_4/CB from their individual CV curves (Fig. S9c, ESI†), indicating the better electrical conductivity after the introduction of carbonaceous materials. The superiority of Co_3O_4/r-GO towards the pristine Co_3O_4 and Co_3O_4/CB is also reflected in the longest discharge time under galvanostatic charge–discharge testing (Fig. S9d, ESI†). Based on these two comparisons, it can be derived that our unique hybrid architecture can (1) improve the electrical conductivity of the overall electrode to a higher level; (2) make full use of both active material and "conducting matrix" by assigning r-GO platelets to almost every single scroll. The appearance of an extra pair of redox peaks (0.33/0.19 V, which can be attributed to the redox transition of Co^{2+}/Co^{3+}[38]) in the CV curves of Co_3O_4/r-GO further implies the improved electrochemical activity of the Co_3O_4/r-GO composite (Fig. 3c and Fig. S9c, ESI†). In addition, the cyclability of Co_3O_4/r-GO and Co_3O_4 is demonstrated as well at a relatively high scan rate of

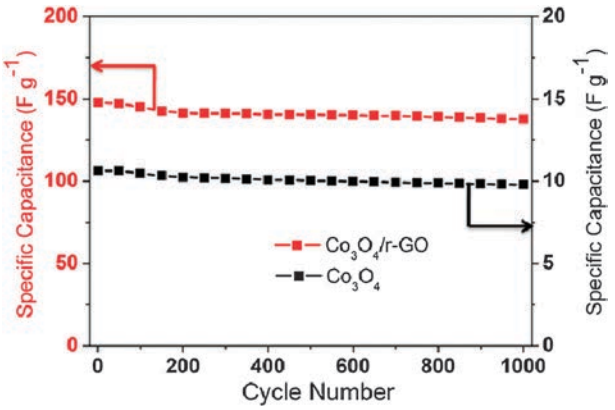

Fig. 4 Average specific capacitance *versus* the cycle number of the Co_3O_4 and Co_3O_4/r-GO at a scan rate of 20 mV s^{-1}.

20 mV s^{-1}. The Co_3O_4/r-GO composite still shows a slightly better retention of 93% than that of Co_3O_4 (91%) after 1000 cycles (Fig. 4).

In summary, we have demonstrated a unique Co_3O_4/r-GO scrolled structure prepared by a facile two-step surfactant-assisted method. Almost every single Co_3O_4 scroll is detected to connect with the r-GO platelets, thus leading to remarkable electrochemical performances in terms of high specific capacitance and good rate capability. Our encouraging results offer a new concept of integration mode between graphene derivatives and other materials, which is believed to be helpful in developing multifunctional graphene composites for potential applications.

This work is supported by the Singapore National Research Foundation under NRF RF Award No. NRF-RF2010-07 and MOE Tier 2 MOE2009-T2-1-037.

Notes and references

1 M. Winter and R. J. Brodd, *Chem. Rev.*, 2004, **104**, 4245–4270.
2 P. Simon and Y. Gogotsi, *Nat. Mater.*, 2008, **7**, 845–854.
3 J. M. Tour, C. Kittrell and V. L. Colvin, *Nat. Mater.*, 2010, **9**, 871–874.
4 R. Kotz and M. Carlen, *Electrochim. Acta*, 2000, **45**, 2483–2498.
5 M. D. Stoller, S. J. Park, Y. W. Zhu, J. H. An and R. S. Ruoff, *Nano Lett.*, 2008, **8**, 3498–3502.
6 T. Y. Kim, H. W. Lee, M. Stoller, D. R. Dreyer, C. W. Bielawski, R. S. Ruoff and K. S. Suh, *ACS Nano*, 2010, **4**, 436–442.
7 Y. W. Zhu, S. Murali, M. D. Stoller, A. Velamakanni, R. D. Piner and R. S. Ruoff, *Carbon*, 2010, **48**, 2118–2122.
8 M. Kaempgen, C. K. Chan, J. Ma, Y. Cui and G. Gruner, *Nano Lett.*, 2009, **9**, 1872–1876.
9 C. C. Hu, K. H. Chang, M. C. Lin and Y. T. Wu, *Nano Lett.*, 2006, **6**, 2690–2695.
10 R. Liu and S. B. Lee, *J. Am. Chem. Soc.*, 2008, **130**, 2942–2943.
11 L. Hu, M. Pasta, F. L. Mantia, L. Cui, S. Jeong, H. D. Deshazer, J. W. Choi, S. M. Han and Y. Cui, *Nano Lett.*, 2010, **10**, 708–714.
12 H. L. Wang, H. S. Casalongue, Y. Y. Liang and H. J. Dai, *J. Am. Chem. Soc.*, 2010, **132**, 7472–7477.
13 H. L. Wang, L. F. Cui, Y. A. Yang, H. S. Casalongue, J. T. Robinson, Y. Y. Liang, Y. Cui and H. J. Dai, *J. Am. Chem. Soc.*, 2010, **132**, 13978–13980.
14 Y. Y. Liang, M. G. Schwab, L. J. Zhi, E. Mugnaioli, U. Kolb, X. L. Feng and K. Mullen, *J. Am. Chem. Soc.*, 2010, **132**, 15030–15037.
15 Z. S. Wu, W. C. Ren, L. Wen, L. B. Gao, J. P. Zhao, Z. P. Chen, G. M. Zhou, F. Li and H. M. Cheng, *ACS Nano*, 2010, **4**, 3187–3194.
16 D. H. Wang, D. W. Choi, J. Li, Z. G. Yang, Z. M. Nie, R. Kou, D. H. Hu, C. M. Wang, L. V. Saraf, J. G. Zhang, I. A. Aksay and J. Liu, *ACS Nano*, 2009, **3**, 907–914.
17 S. M. Paek, E. Yoo and I. Honma, *Nano Lett.*, 2009, **9**, 72–75.
18 D. H. Wang, R. Kou, D. Choi, Z. G. Yang, Z. M. Nie, J. Li, L. V. Saraf, D. H. Hu, J. G. Zhang, G. L. Graff, J. Liu, M. A. Pope and I. A. Aksay, *ACS Nano*, 2010, **4**, 1587–1595.
19 G. M. Zhou, D. W. Wang, F. Li, L. L. Zhang, N. Li, Z. S. Wu, L. Wen, G. Q. Lu and H. M. Cheng, *Chem. Mater.*, 2010, **22**, 5306–5313.
20 L. S. Zhang, L. Y. Jiang, H. J. Yan, W. D. Wang, W. Wang, W. G. Song, Y. G. Guo and L. J. Wan, *J. Mater. Chem.*, 2010, **20**, 5462–5467.
21 C. Xu, X. Wang, J. W. Zhu, X. J. Yang and L. Lu, *J. Mater. Chem.*, 2008, **18**, 5625–5629.
22 Z. S. Wu, D. W. Wang, W. Ren, J. Zhao, G. Zhou, F. Li and H. M. Cheng, *Adv. Funct. Mater.*, 2010, **20**, 3595–3602.
23 S. B. Yang, X. L. Feng, S. Ivanovici and K. Mullen, *Angew. Chem., Int. Ed.*, 2010, **49**, 8408–8411.
24 Y. Xu, H. Bai, G. Lu, C. Li and G. Shi, *J. Am. Chem. Soc.*, 2008, **130**, 5856–5857.
25 W. S. Hummers and R. E. Offeman, *J. Am. Chem. Soc.*, 1958, **80**, 1339–1339.
26 S. Stankovich, D. A. Dikin, G. H. B. Dommett, K. M. Kohlhaas, E. J. Zimney, E. A. Stach, R. D. Piner, S. T. Nguyen and R. S. Ruoff, *Nature*, 2006, **442**, 282–286.
27 S. Stankovich, R. D. Piner, X. Q. Chen, N. Q. Wu, S. T. Nguyen and R. S. Ruoff, *J. Mater. Chem.*, 2006, **16**, 155–158.
28 L. M. Viculis, J. J. Mack and R. B. Kaner, *Science*, 2003, **299**, 1361.
29 X. Xie, L. Ju, X. F. Feng, Y. H. Sun, R. F. Zhou, K. Liu, S. S. Fan, Q. L. Li and K. L. Jiang, *Nano Lett.*, 2009, **9**, 2565–2570.
30 X. Chen, X. Sun and Y. Li, *Inorg. Chem.*, 2002, **41**, 4524–4530.
31 G. Zhang, S. Sun, R. Li, Y. Zhang, M. Cai and X. Sun, *Chem. Mater.*, 2010, **22**, 4721–4727.
32 X. C. Jiang, Y. Xie, J. Lu, L. Y. Zhu, W. He and Y. T. Qian, *Adv. Mater.*, 2001, **13**, 1278–1281.
33 O. G. Schmidt and K. Eberl, *Nature*, 2001, **410**, 168.
34 W. Zhu, W. Z. Wang, H. L. Xu, L. Zhou, L. H. Zhang and J. L. Shi, *Cryst. Growth Des.*, 2006, **6**, 2804–2808.
35 W. X. Zhang, X. G. Wen, S. H. Yang, Y. Berta and Z. L. Wang, *Adv. Mater.*, 2003, **15**, 822–825.
36 M. D. Stoller and R. S. Ruoff, *Energy Environ. Sci.*, 2010, **3**, 1294–1301.
37 V. Khomenko, E. Frackowiak and F. Beguin, *Electrochim. Acta*, 2005, **50**, 2499–2506.
38 L. Cui, J. Li and X. G. Zhang, *J. Appl. Electrochem.*, 2009, **39**, 1871–1876.